

PAPER

Impurity pinch generated by trapped particle driven turbulence

To cite this article: K Lim *et al* 2020 *Plasma Phys. Control. Fusion* **62** 095018

View the [article online](#) for updates and enhancements.



IOP | ebooks™

Bringing together innovative digital publishing with leading authors from the global scientific community.

Start exploring the collection—download the first chapter of every title for free.

Impurity pinch generated by trapped particle driven turbulence

K Lim¹, E Gravier¹, M Lesur¹, X Garbet², Y Sarazin² and J Médina¹

¹ Institut Jean Lamour (IJL), UMR 7198 CNRS - Université de Lorraine, 54000 Nancy, France

² CEA, IRFM, F-13108 Saint-Paul-Lèz-Durance, France

E-mail: kyungtak.lim@univ-lorraine.fr

Received 17 February 2020, revised 22 June 2020

Accepted for publication 6 July 2020

Published 5 August 2020



CrossMark

Abstract

Impurity turbulent transport in tokamak plasmas is investigated in the case of trapped ion mode (TIM) and trapped electron mode (TEM) using a non-linear bounce-averaged gyrokinetic model. In particular, we focus on the thermo-diffusive pinch and the curvature-driven pinch observed in non-linear simulations. Thermodiffusion is analyzed independently of curvature pinch by disabling the latter artificially. A parameter scan shows that the direction of thermodiffusion depends mainly on two factors. First, it depends on the sign of the turbulence phase velocity, and the resulting transport is inward in the case of TEM whereas it is outward in the case of TIM. Second, it depends on the sign of the impurity temperature gradient. Moreover, the magnitude of the thermodiffusion tends to decrease with respect to the impurity charge Z , while it is proportional to the intensity of background turbulence. Lastly, the direction of the curvature pinch is investigated as a function of the magnetic shear. The results of non-linear simulations are compared with quasi-linear theory. The Kubo number is calculated for our non-linear simulations to justify this comparison. Quasi-linear theory is found to be in qualitative agreement with our gyrokinetic numerical observations.

Keywords: gyrokinetic, impurity transport, turbulence

(Some figures may appear in colour only in the online journal)

1. Introduction

Since its discovery, numerous models have been designed to explain for turbulent transport driven by micro-instabilities. It is essential to characterize clearly such enhanced transport, because particle transport across a magnetic field could lead to particle and energy losses. This undesired effect would seriously reduce the confinement time, a factor which must be considered in the conception of future fusion devices. In addition, when this transport is coupled to impurities in plasma, an even worse situation can arise, such as impurity accumulation in the core. Sources of impurities are diverse since they might be added naturally, deliberately or inevitably. For example, α -particles (He) are produced by fusion reactions while Argon (Ar) and Neon (Ne) can be injected on purpose to relieve heat fluxes on plasma facing components (PFC). Recently, Tungsten (W) is in the spotlight for future PFC and it can be sputtered from the wall due to uncontrolled edge localized modes and unmitigated disruptions [1].

The presence of impurities in plasma has negative effects on fusion viability, and these can be summarized in two major ways. First, increasing impurity concentration dilutes the deuterium (D) and tritium (T) fuel, then it reduces the plasma fusion efficiency. Second, high- Z impurities are not completely ionized even at the core temperature of tokamaks. These partially ionized particles undergo further ionization and radiate considerable plasma energy. For instance, it is well known that even at a concentration as low as 3×10^{-5} [2], accumulated tungsten can lead to a radiative collapse of the core plasma. Consequently, it is important to investigate the dynamics of impurity particles under our control and avoid their accumulation in the core.

The turbulent impurity transport is composed of a diffusive part and a convective part [3]. For the diffusive part, numerous studies have been carried out and some of these produce results in agreement with experiments [4]. The physics of convective part, however, still needs to be fully understood. For example, it has been suggested that the poloidal asymmetry of

impurity distribution induced by turbulence or external heating systems might change the convective velocity by an order of magnitude, even its direction [5]. Also, the centrifugal force driven by the neutral beam injection could possibly change the magnitude and the direction of the convective velocity in case of a strongly rotating plasma [6].

To determine the accurate parametric dependence of the impurity convective flux is a demanding task because of the non-linear nature of instabilities driven by turbulence. Nevertheless, recently various results have been achieved explaining the impurity transport in tokamaks. For example, fluid models [7] or gyrokinetic models [8] containing realistic tokamak geometry [9], auxiliary heating [10], collisionality [11], rotational shear [12], toroidal rotation [13], poloidal asymmetries [14, 15], turbulent or neoclassical contribution [16, 17], have been successfully investigated. However, these models have been usually tested with their own assumptions to alleviate the numerical cost and the mathematics. Such assumptions sometimes made it hard to understand the convective flux clearly. Therefore, an integrated model with less assumptions should be tested for a more understanding of the convective flux.

In this work, we investigate the unambiguous parametric dependencies of impurity pinch driven by trapped particle turbulence. More accurately, the effect of trapped particle driven mode on turbulent impurity particle flux is studied by means of global non-linear gyrokinetic code. To restrict our study solely to a turbulent case, only light-impurity will be studied actively. Effectively, impurity collisionality increases with charge and therefore neoclassical transport becomes dominant in the heavy impurity case. Over the whole of our study, the concentration of impurity \mathcal{C}_s is fixed at the trace limit, which means the presence of impurities does not change the nature of the background plasma turbulence. The quasi-linear (QL) derivation of pinch terms from a non-linear full- f gyrokinetic model is presented in this paper. Especially, the thermodiffusion and the curvature pinch in trapped ion/electron dominant mode (TIM/TEM) are studied separately. As we mentioned above, the direction of impurity flux is an important issue, because inward flux can lead to accumulation. Thus, it might extinguish the burning plasma. Thermodiffusion for impurity is expected to be outward/inward when the ion/electron mode is dominant and its magnitude tends to decrease with the impurity charge [7]. The curvature pinch does not depend on the charge nor on the background turbulence and is usually directed inward unless the magnetic shear s is strongly negative. These results are demonstrated numerically and compared with QL theory. QL theory qualitatively reproduces our gyrokinetic numerical observations. Furthermore, the Kubo number for each simulations is calculated to validate the main approximation used to derive QL theory.

The non-linear TERESA code is based on a semi-Lagrangian numerical scheme [18] where the distribution function f_s of each species evolves in a collisionless plasma. This code enables the study of a trapped particle-driven mode such as TIM/TEM while treating the passing particles adiabatically. Considering only trapped particles allows different time scale dynamics to be filtered. For this reason, the TERESA

code can operate with multiple species at low numerical cost [19]. Further information about the code will be presented in the next section. In this paper, we restrict ourselves to the case of electrostatic turbulence in which magnetic perturbation can be negligible.

The paper is organized as follows. Section 2 describes the gyrokinetic TERESA model used in this work. In section 3, several components of particle flux such as thermodiffusion and curvature pinch are derived using the QL theory and the validity of QL approximation is tested. The non-linear numerical results are presented in section 4 and the paper ends with a conclusion.

2. Numerical model

The TERESA (Trapped Element REduction in Semi Lagrangian Approach) code is based on an electrostatic bounce averaged gyrokinetic model [20–23]. TEM and TIM are instabilities that are characterized by frequencies ω of the order of ω_d , the precession frequency. And this latter frequency is smaller than ω_b , the bounce frequency, which itself is smaller than the cyclotron frequency ω_c . Therefore, it is possible to gyro-average and bounce-average the Vlasov equation, thus filtering out the fast cyclotron and bounce frequencies, and the small space scales ρ_c (gyro-radius) and δ_b (banana width). These assumptions lead to a reduction of dimensionality, from 5D gyrokinetics, to 4D gyrobounce-gyrokinetics [24]. Therefore, a low frequency mode of trapped particles such as TIM and TEM can be described via the 4D-Vlasov equation. In this code, the trapped particles are treated kinetically for both ions and electrons, while passing particles are treated adiabatically.

Periodical motion of trapped particles in the dynamic system is well-suited to the application of action-angle variables. Thus, the evolution of the distribution function f_s is described by two variables (ψ, α) respectively (i) the magnetic flux ψ (with $d\psi = -B_\theta R_0 dr$), which is taken as a radial coordinate in this paper and (ii) the toroidal precession angle $\alpha = \varphi - q\theta$ where φ is the toroidal angle, q is the safety factor and θ is the poloidal angle. The axisymmetric toroidal magnetic configuration $\mathbf{B}(\psi, \theta) = B_{\min}(\psi)(1 + \frac{r}{R} \cos \theta)$ is used where B_{\min} is the minimal value of the magnetic field at a given ψ and at $\theta = 0$. Furthermore, we choose an inverse aspect ratio $a/R_0 = 0.1$ and a safety factor $q(r) = 1.2 + 3(r/a)^2$. Moreover, two parameters (i) the particle kinetic energy E and (ii) the trapping parameter $\kappa = \sqrt{\frac{1-\lambda}{2\varepsilon\lambda}} = \sin(\frac{\theta_0}{2})$ with $\lambda = \mu B_{\min}/E$, θ_0 the pitch angle and $\varepsilon = a/R_0$ the inverse aspect ratio of tokamak are used to parallelize the numerical code.

After applying the gyro-bounce average operator \mathcal{J} and the angle-action variables, our reduced Vlasov equation can be written:

$$\frac{\partial f_s}{\partial t} - [\mathcal{J}_{0,s}\phi, f_s]_{\alpha, \psi} + \frac{\Omega_d E}{Z_s} \frac{\partial f_s}{\partial \alpha} = 0 \quad (1)$$

where f_s is the gyro-bounce averaged particle distribution function for species $s = i, e, z$ and ϕ is the gyro-bounce averaged plasma potential. The Poisson brackets are defined as

$[g, h] = \partial_\alpha g \partial_\psi h - \partial_\alpha h \partial_\psi g$ and $\Omega_d = \frac{Z_s \omega_{d,s}}{E}$ where the toroidal precession frequency $\omega_{d,s}$ is defined:

$$\omega_{d,s} = \frac{q}{a} \frac{E}{q_s B_{\min} R_0} \bar{\omega}_d \quad \text{with} \quad \bar{\omega}_d = \left(\frac{2\mathcal{E}(\kappa)}{\mathcal{K}(\kappa)} - 1 + 4s_0 \left(\frac{\mathcal{E}(\kappa)}{\mathcal{K}(\kappa)} + \kappa - 1 \right) \right) \quad (2)$$

Here, q_s is the electric charge of the species s and B_{\min} is the minimal strength of the magnetic field on a field line. $\mathcal{E}(\kappa)$, $\mathcal{K}(\kappa)$ represent respectively first and second kind elliptic functions and s_0 is the magnetic shear. Note that, for positive and finite s_0 , both $\mathcal{E}(\kappa)$ and $\mathcal{K}(\kappa)$ weakly depend on the trapping parameter κ , except for a small region close to the trapped-passing boundary at $\kappa \approx 1$. In the reminder of the paper, we will further consider deeply trapped particles only, for which $\kappa \approx 0$. In this case, $\bar{\omega}_d$ is simply a constant which turns out to be positive, and which we shall note $\bar{\omega}_{d0}$ hereafter.

The gyro-bounce average operator can be expressed as a Taylor expansion:

$$\mathcal{J}_{0,s} \simeq \left(1 + \frac{E}{T_{0,s}} \frac{\delta_{b0,s}^2}{4} \partial_\psi^2 \right) \left(1 + \frac{E}{T_{0,s}} \frac{q^2 \rho_{c0,s}^2}{4a^2} \partial_\alpha^2 \right) \quad (3)$$

where $\rho_{c0,s}$ and $\delta_{b0,s}$ are the Larmor radius and the banana width.

Note that the precession frequency $\omega_{d,s}$ does not depend on the mass but on the charge. As a result, the toroidal precession frequency for hydrogen ions and electrons is of the same order, allowing us to study TIM/TEM dynamics with reasonable computation times.

The self-consistency of the model is assured by the quasi-neutrality equation between species. Unlike other gyrokinetic codes, the TERESA code is capable of running multiple species at the same time with less numerical constraints. This advantage makes it possible to consider several impurities in one simulation. The normalized quasi-neutrality equation for N-species can be expressed:

$$\frac{2}{\sqrt{\pi}} \frac{T_{eq,i}}{T_0} \sum_s \left(Z_s C_s \int_0^\infty \mathcal{J}_{0,s} f_s E^{1/2} dE \right) = C_{ad} (\phi - \epsilon_\phi < \phi >_\alpha) - C_{pol} \sum_s C_s \tau_s Z_s^2 \Delta_s \phi \quad (4)$$

where $C_s = N_s/N_{0,e}$ is the concentration of the species s (N_s is the population s density, $N_{eq} = N_{0,e}$ is the equilibrium density and the quasi-neutral condition satisfies $\sum_s Z_s N_s = 0$), $C_{pol} = e\omega_0 L_\psi / T_0$ is the coefficient for finite Larmor radius effects where $\omega_0 = \frac{T_0}{eR_0^2 B_\theta}$ is the reference ion toroidal precession frequency and $C_{ad} = C_{pol} \frac{1-f_T}{f_T} \sum_s (Z_s^2 C_s \tau_s)$ is the adiabatic coefficient for passing particles where f_T is the fraction of trapped particles and $\tau_s = T_{eq,i} / T_s$. The operator Δ_s is defined as $\Delta_s = \left(\frac{q\rho_{c0,s}}{a} \right)^2 \partial_\alpha^2 + \delta_{b0,s}^2 \partial_\psi^2$ and $\epsilon_\phi = \sum_s \tau_s C_s Z_s^2 \epsilon_{\phi,s} / (\sum_s \tau_s C_s Z_s^2)$ is an ad-hoc coefficient which controls the magnitude of the axisymmetric potential $< \phi >_\alpha$ (Zonal flows). Also notice that the integral over the velocity space in equation (4) simply

Table 1. Normalization of physical quantities. Here $\omega_0 = T_0 / eR_0^2 B_\theta$ is a typical precession frequency of strongly trapped ions at $E = T_0$. N_0 and T_0 are arbitrary normalizing ion density and temperature such that $\hat{N} = \hat{T} = 1$ at $\hat{\psi} = 0$. $L_\psi = aR_0 B_\theta$ is the radial size of the simulation box in magnetic flux units.

Quantity	e.g.	Normalization
Time	t, ω_{-1}	$\hat{t} = \omega_0 t$
Length	r	$\hat{r} = r(B_\theta / q_0 L_\psi)^{1/2}$
Poloidal magnetic flux	$\psi, a, \rho_0, \delta_b$	$\hat{\psi} = \psi / L_\psi$
Electric potential perturbation	ϕ	$\hat{\phi} = \phi / (\omega_0 L_\psi)$
Energy	E	$\hat{E} = E / T_0$
Density	N	$\hat{N} = N / N_0$
Temperature	T	$\hat{T} = T / T_0$
Distribution function	f	$\hat{f} = \frac{1}{N_0} \left(2\pi \frac{T_0}{m} \right)^{3/2} f$

Table 2. Larmor radius ρ_s and banana widths δ_s used for the non-linear simulations. The values of the Larmor radius are at the thermal velocity, and the approximation of constant orbit width is used.

ρ_D	ρ_e	ρ_{He}	δ_D	δ_e	δ_{He}
10^{-2}	2×10^{-4}	7.07×10^{-3}	10^{-1}	2×10^{-3}	7.07×10^{-2}

reduces to an integral over the energy since the trapping parameter κ is taken equal to 0 in this paper.

Furthermore an artificial buffer diffusion has been implemented at both sides of the simulation box to prevent numerical instabilities at the boundary region. The value of the buffer coefficient diffusion and its width were chosen not to disturb plasma transport at the core region. Its shape is as follows:

$$D_{\text{buffer}}(\psi) = D_0 \left[2 - \tanh \frac{\psi - \psi_0}{L_D} + \tanh \frac{L_\psi - \psi_0 - \psi}{L_D} \right] \quad (5)$$

where the buffer coefficient diffusion $D_0 = 10^{-3}$, the width of the buffer region $\psi_0 = 0.15$ and the edge smoothness $L_D = 0.02$.

All the quantities presented above are normalized as listed in table 1 and the input Larmor radius and banana widths are listed in table 2. In our models, all frequencies are normalized to the ion precession frequency ω_0 at the typical temperature T_0 (in tokamaks the ion precession frequency is of the order 1000 rad/s⁻¹) with the $\rho^* = 1/100$ and $v_{Ti} \sim c_s$ (ion sound speed) for $T_e = T_i$. Hereafter, hat-notation will be omitted for the sake of equation simplicity and all the results presented in this paper will also be normalized values.

3. Impurity pinch

In general, it is customary to decompose the total particle flux due to turbulence into the sum of the diffusive and convective parts [3], as follows.

$$\Gamma_z = -D_z \nabla N_z + N_z V_z \quad (6)$$

where D_z is a diffusion coefficient and V_z is a convective (pinch) velocity. This seemingly simple equation results from

complex turbulent effects hidden in the coefficient D_z and pinch velocity V_z . In spite of their strong correlations with other parameters and turbulence, a QL theory has been used to express the impurity flux analytically and a more detailed form of the pinch velocity V_z is derived in section 3.1. In addition, a useful method has been designed for the study of the convective part separately from the diffusive part with non-linear simulations and this method will be presented in section 3.3.

3.1. QL impurity transport

Turbulent particle transport can be addressed by means of the QL model in the framework of weak turbulence. The QL theory has already been tested by several authors to compute turbulent impurity particle flux [7, 25–27] and recently the TERESA code was found to reproduce qualitatively particle/heat flux in agreement with QL predictions [28, 29]. In this section, as an extension of previous work, the general Γ_z formula of impurity particle flux is derived analytically with the help of a kinetic approach of QL theory (fluid approach is also presented in appendix A) where the presence of the thermodiffusion pinch and the curvature pinch is verified.

First, the bounce-averaged distribution function f satisfies the Vlasov equation:

$$\frac{\partial f}{\partial t} - [\mathcal{J}\phi, f] + \frac{\Omega_d E}{Z} \frac{\partial f}{\partial \alpha} = 0 \quad (7)$$

Here, the distribution function f and the electric potential ϕ can be split into perturbed and unperturbed parts with the assumptions $\tilde{f} \ll f_{eq}$ and $\tilde{\phi}_{eq} = 0$.

$$\begin{aligned} f &= f_{eq}(\psi, E, t) + \tilde{f} \\ \phi &= \tilde{\phi} \end{aligned} \quad (8)$$

the Maxwellian distribution function f_{eq} is defined:

$$f_{eq} = \frac{N_{eq}}{T_{eq}^{3/2}} \exp\left(-\frac{H_{eq}}{T_{eq}}\right) \quad (9)$$

where $H_{eq} = E(1 + e\Omega_d\psi)$.

Assuming the amplitudes are small enough that frequency and growth rates of the modes can be described by linear theory, equation (7) can be rewritten by keeping only first order terms of the perturbed part:

$$\frac{\partial \tilde{f}}{\partial t} - \frac{\partial \mathcal{J}\phi}{\partial \alpha} \frac{\partial f_{eq}}{\partial \psi} + \frac{\Omega_d E}{Z} \frac{\partial \tilde{f}}{\partial \alpha} = 0 \quad (10)$$

Then, we apply spatial averages of equation (7) over α ($\langle \cdot \rangle = \frac{1}{2\pi} \int d\alpha$). By combining it with equation (10) and neglecting terms with an order higher than 2, the above equation is written as:

$$\frac{\partial f_{eq}}{\partial t} = \frac{\partial}{\partial \psi} \langle \tilde{f} \frac{\partial \mathcal{J}\phi}{\partial \alpha} \rangle \quad (11)$$

Now the above equation can be expressed by means of the Fourier decomposition $\tilde{f}_s = \sum_n \tilde{f}_n e^{i(n\alpha - \omega t)}$ and $\tilde{\phi} = \sum_n \phi_n e^{i(n\alpha - \omega t)}$ where $\omega = \omega_r + i\gamma$ is composed of the real

Table 3. Impurity pinch direction. Reproduced from [26], with the permission of AIP Publishing.

	Thermodiffusion	Curvature pinch
Trapped Ion Mode (TIM)	Outward	Inward (Outward if $s \ll 0$)
Trapped Electron Mode (TEM)	Inward	

frequency and the growth rate. After some arrangement, we finally find the relationship between the perturbed distribution function and the perturbed potential.

$$f_n = \frac{\kappa_n + \left(\frac{E}{T_{eq}} - \frac{3}{2}\right)\kappa_T - e\Omega_d \frac{E}{T_{eq}}}{\frac{\omega}{n} - \frac{\Omega_d E}{Z}} f_{eq} \mathcal{J}\phi_n \quad (12)$$

where $\kappa_n = -\frac{1}{N_{eq}} \frac{dN_{eq}}{d\psi}$, $\kappa_T = -\frac{1}{T_{eq}} \frac{dT_{eq}}{d\psi}$ and equation (11) yields:

$$\frac{\partial \langle N \rangle_\alpha}{\partial t} + \frac{\partial \Gamma_z}{\partial \psi} = 0 \quad (13)$$

Here, the Γ_z being the impurity transport in the radial direction:

$$\begin{aligned} \Gamma_z &= \sum_n \int (n\mathcal{J}\phi_n)^2 \frac{\gamma}{(\omega_r - n\frac{\Omega_d E}{Z})^2 + \gamma^2} \\ &\quad \left[\kappa_{nz} + \left(\frac{E}{T_{eq}} - \frac{3}{2}\right)\kappa_{Tz} - e\Omega_d \frac{E}{T_{eq}} \right] f_{eq} \sqrt{E} dE \end{aligned} \quad (14)$$

The above equation can be recast as:

$$\Gamma_z = D_z N_z \kappa_{nz} + C_T \kappa_{Tz} + C_p \quad (15)$$

The first term in equation (15), proportional to κ_{nz} , is a diffusive part of the impurity flux. The second term is the thermodiffusion $C_T \kappa_{Tz}$ which stems from the inherent temperature gradient in tokamak [30]. It should be noted that the temperature gradient in the thermodiffusion term depends on the temperature gradient of the transported species and not on the temperature gradient driving the turbulence [7]. In addition, the sign of coefficient C_T in equation (15) depends on the phase velocity. For example, the direction of thermodiffusion is inward when turbulence is dominated by electrons and outward when turbulence is dominated by ions. Usually, the magnitude of C_T tends to decrease for high-Z impurities [7, 16]. Thus in the case of high charge impurities such as tungsten (W), the C_T impact decreases significantly. The last term is the curvature pinch C_p which is proportional to magnetic field curvature. It is originated from the perpendicular compression of $E \times B$ drift velocity. This term is proportional to $\nabla q/q$ (q is the safety factor) leading to an inward direction except for reversed shear plasma [25]. Usually, another pinch exists, the parallel compression pinch [10], which is proportional to Z/A where A is the impurity mass number, such that $m_z = Am_H$ and has a direction opposed to thermodiffusion. Thus it is inward for ion dominated turbulence and outward for electron dominated turbulence. This term cannot be accounted for in TERESA simulations because the parallel electric force is neglected. Thus parallel dynamic is not considered.

3.2. Validity of the QL approximations

Before performing a comparison of the results given by the non-linear simulations with those given by the QL theory, here we discuss the validity of the QL theory. The two main approximations, specifically (i) a weak fluctuation level ($\delta f \ll f$), (ii) no trapped particles in the saturated potential field, are usually used to derive the gyrokinetic QL fluxes. The first approximation which assume a small level of amplitude of the fluctuations is usually satisfied in the core of tokamaks. Thus, the second approximation is often tested for the validity of QL theory.

To demonstrate the second approximation, a dimensionless number, the so-called Kubo number \mathcal{K} , has been introduced in the literature. The Kubo number is defined as follows [31]:

$$\mathcal{K} = \frac{\tau_{ac}}{\tau_f} \quad (16)$$

Here, τ_{ac} represents the wave-particle interaction time. This can be obtained from the non-linear simulations by using an autocorrelation time of the maximal saturated potential ϕ_{\max} (figure 1). And τ_f is the flight time of a particle along the electric potential structure. The ratio between these two times should be lower than 1 ($\mathcal{K} < 1$) in order that the particles are not trapped in the potential. In this paper, an analytical approach to obtain τ_f has been applied by assuming that particles follow a circle trajectory around the maximal electric potential ϕ_{\max} .

First of all, we suppose the simple form of electric potential $\phi = \phi_0 \cos(n\alpha) \cos(k\psi)$ where each n, k represents the mode number in α, ψ direction and ϕ_0 is the maximal electric potential. Putting $x = n\alpha$ and $y = k\psi$, we can find the orbit of particles near the points $x = y = 0$ as follows due to the second order of expansion:

$$\frac{\phi}{\phi_0} = 1 - \frac{x^2 + y^2}{2} \quad (17)$$

Using the Hamiltonian relation in the angle-action coordinates $\frac{dJ_3}{dt} = -\frac{\partial H}{\partial \alpha}$ and $\frac{d\alpha}{dt} = \frac{\partial H}{\partial J_3}$, we can find a relation:

$$\begin{aligned} \frac{d\psi}{dt} &= -\frac{\partial \phi}{\partial \alpha} \\ \frac{d\alpha}{dt} &= \frac{\partial \phi}{\partial \psi} \end{aligned} \quad (18)$$

where we assumed $E = 0$ in the Hamiltonian $H = E(1 + q_s \Omega_d \psi) + q_s \phi$ and $J_3 = q_s \psi$. The above equation (18) can be rewritten in terms of x and y :

$$\begin{aligned} \frac{dx}{dt} &= nk \frac{\partial \phi}{\partial y} \\ \frac{dy}{dt} &= -nk \frac{\partial \phi}{\partial x} \end{aligned} \quad (19)$$

It can be shown that equation (19) satisfies the relation $x \frac{dx}{dt} + y \frac{dy}{dt} = 0$ which means the orbit of particles is a circle $x^2 + y^2 =$

r^2 . Now, we apply the polar coordinates $x = r \cos \theta$ and $y = r \sin \theta$ for equation (19):

$$\begin{aligned} \frac{dx}{dt} &= -r \frac{d\theta}{dt} \sin \theta = nk \frac{\partial \phi}{\partial y} = -nk \phi_0 r \sin \theta \\ \frac{dy}{dt} &= r \frac{d\theta}{dt} \cos \theta = -nk \frac{\partial \phi}{\partial x} = nk \phi_0 r \cos \theta \end{aligned} \quad (20)$$

From the above equation, we can find a relation $\frac{d\theta}{dt} = nk \phi_0$. Finally, we can calculate the flight time for a particle to travel along the circle:

$$\tau_f = \int dt = \int \left(\frac{d\theta}{dt} \right)^{-1} d\theta = \frac{2\pi}{nk \phi_0} \quad (21)$$

In figure 2, the Kubo number \mathcal{K} is calculated from non-linear gyrokinetic simulations with a scan of background temperature profile κ_T varying $\kappa_{T_i}, \kappa_{T_e}$ simultaneously. For given plasma parameters, the Kubo number easily exceeds the validity limit $\mathcal{K} < 1$ and the discrepancy gets larger when there is high temperature gradient. This fact reveals that QL approximation easily fails with more unstable plasma (high κ_T) and it converges into the valid limit $\mathcal{K} \sim 1$ by weakening the background instability (low κ_T). Although the Kubo number is not satisfied for our non-linear simulations, some examples have already shown that the QL framework could be applicable even with large Kubo number $\mathcal{K} > 1$ [32, 33].

3.3. Determining pinch velocities from non-linear numerical simulations

To define the pinch contribution in the impurity flux, contributions from the diffusive and convective parts have to be separated. Therefore, it is useful to transform equation (6) into a linear equation of ∇N_z as follows:

$$\frac{\Gamma_z}{N_z} = -D_z \frac{\nabla N_z}{N_z} + V_z = +D_z \kappa_{nz} + V_z \quad (22)$$

with $\kappa_{nz} = -\frac{\nabla N_z}{N_z}$. By doing so, we can not only separate the pinch velocity in equation (22) but also obtain an accurate value of V_z knowing the particle flux Γ_z at different density gradients ∇N_z . Here, we use the impurity particle flux Γ_z averaged over α and it can easily be computed from non-linear gyrokinetic simulations while ∇N_z should be calculated in the turbulent state as the initial value ∇N_z changes during the simulation.

The shaded part of figure 3 shows the beginning of the turbulent state and this region has been chosen on purpose so as to select a correct value of ∇N_z . In figure 3(a), the time evolution of the 10 most unstable modes ϕ_n is represented. The first period $0 < t < 2\omega_0^{-1}$ is linear phase where the turbulence is triggered, but is not entirely developed. The following shaded zone $2\omega_0^{-1} < t < 4\omega_0^{-1}$ indicates where turbulence is evolving toward a relaxation state. Since we focus principally on the part where turbulence is already settled, the shaded region will be appropriate to choose our value of ∇N_z . It can be seen in figure 3(b) that the time cumulative Γ_z increases linearly, therefore it will be possible to evaluate Γ_z accurately.

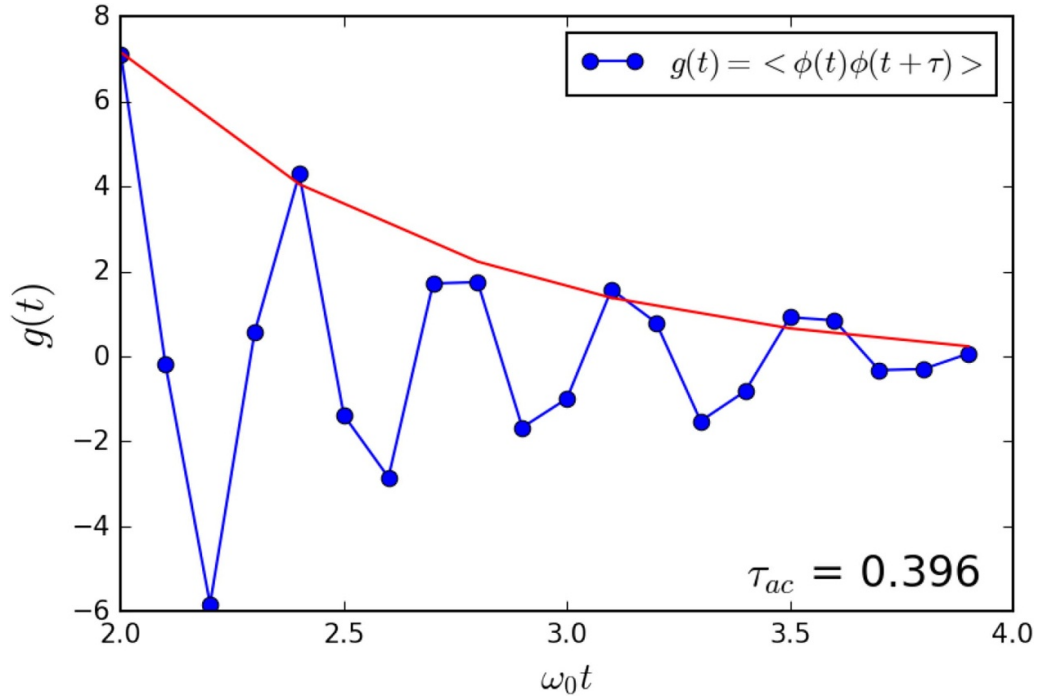


Figure 1. Wave–particle interaction time τ_{ac} obtained by an autocorrelation function $g(\tau)$ of the electric potential in the relaxation state ($2\omega_0^{-1} < t < 4\omega_0^{-1}$) with plasma profiles $\kappa_n = 0.1$ and $\kappa_T = 0.05$. Here, τ_{ac} is equivalent to the decay time of exponential fitting.

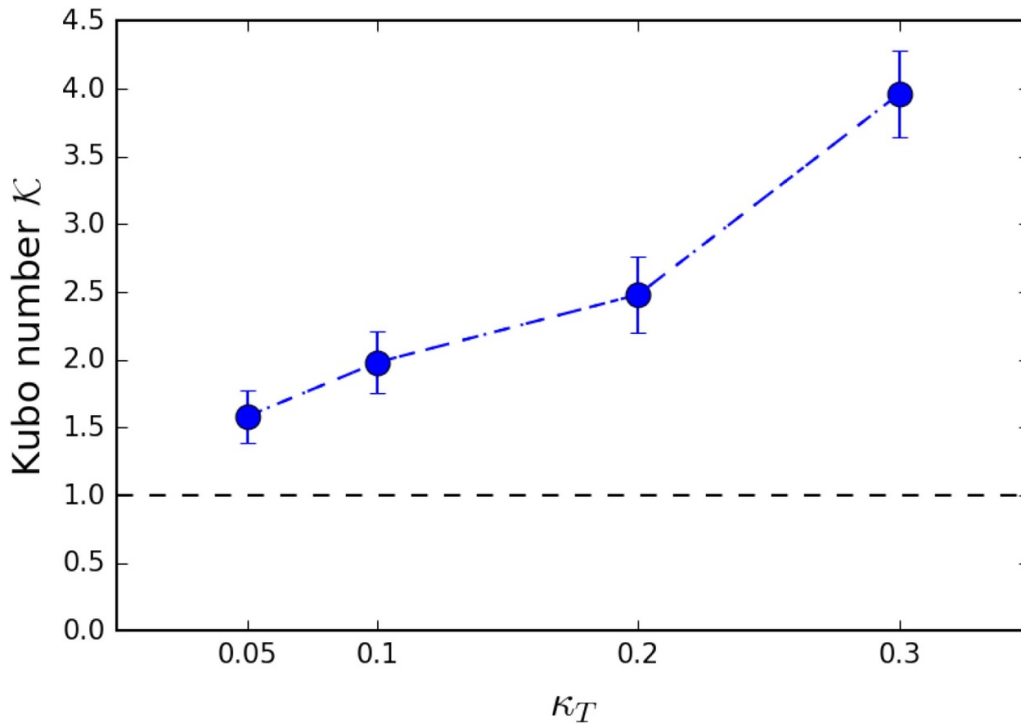


Figure 2. The Kubo number \mathcal{K} is calculated for different background temperature profiles κ_T while density profile is fixed at $\kappa_n = 0.1$.

We need to pay attention to determine the proper value $\kappa_{nz} = -\frac{\nabla N_z}{N_z}$ since the inherent plasma turbulence can modify the initial value of κ_{nz} during simulation. It is shown in figure 4 that the value of the impurity density gradient $\kappa_{nz}(t = 2\omega_0^{-1})$ in turbulent regime is no longer identical to the initial impurity density gradient $\kappa_{nz}(t = 0)$. It is, therefore, necessary to

compute the modified κ_{nz} value in the turbulent regime. As already mentioned, numerical buffer regions are implemented at both edge sides $0 < \psi < 0.15$ and $0.85 < \psi < 1.0$. Thus, only the core region $0.2 < \psi < 0.8$ has been taken into account for the computation of κ_{nz} . It should be noted that in this article $\psi = 0$ stands for the core plasma, and $\psi = 1$ for the plasma

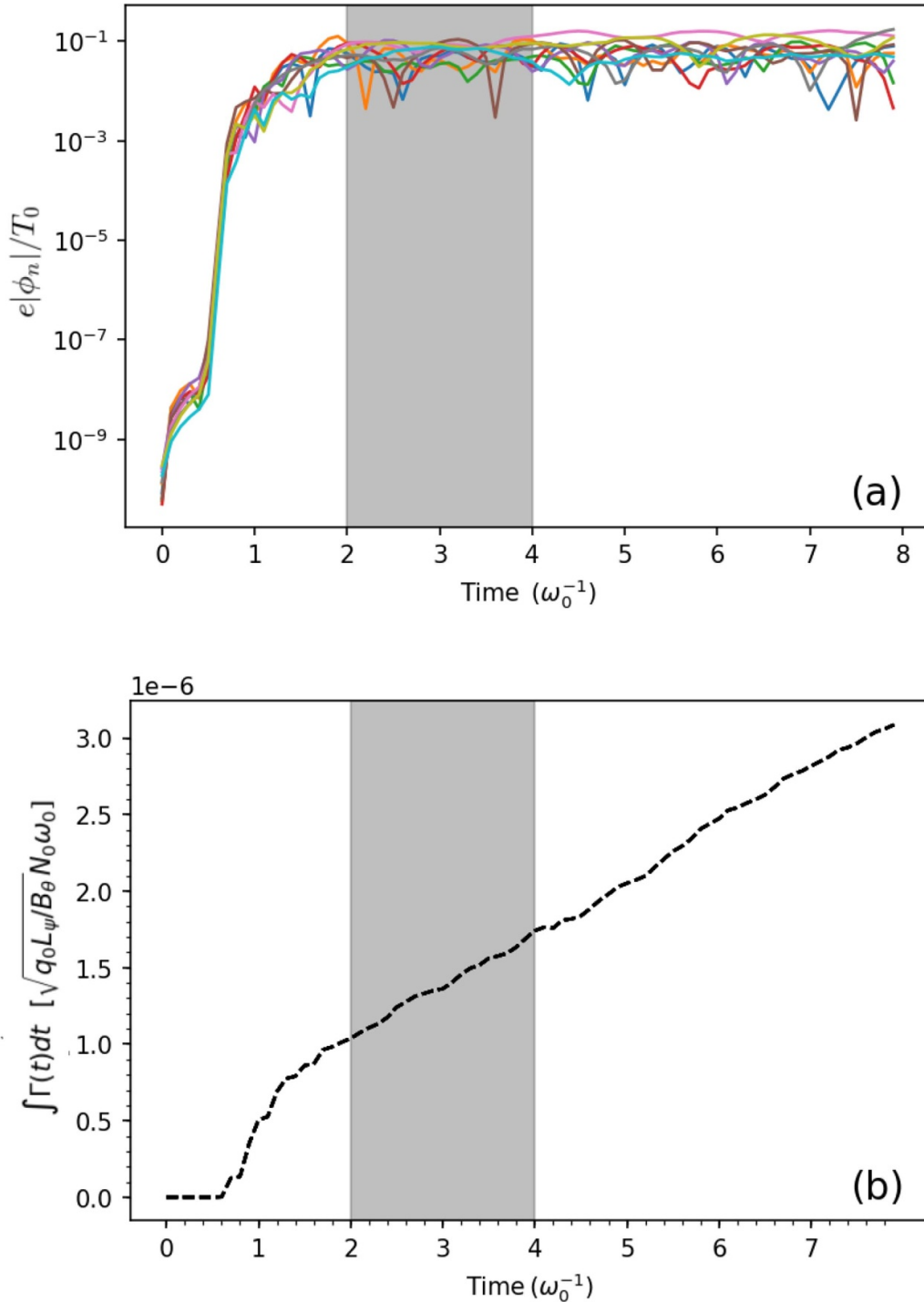


Figure 3. (a) Time evolution of the 10 most unstable ϕ_n modes. (b) Cumulative impurity particle flux Γ_z as a function of time. The shaded region represents the beginning of the turbulent regime and this region is chosen for the study of impurity pinch.

edge, whereas the opposite convention was sometimes used in previous papers using the same TERESA model [28, 34].

Knowing the value of $\kappa_{nz} = -\nabla N_z / N_z$ and the corresponding Γ_z value (Γ_z averaged between $t = 2\omega_0^{-1}$ and $4\omega_0^{-1}$ in figure 3) from the non-linear simulation, we can plot Γ_z / n_z against κ_{nz} , and draw a straight line between multiple pairs $(\kappa_{nz}, \frac{\Gamma_z}{N_z})$, with the help of the linear regression method. As an example of the method, figure 5 shows that a straight line

is drawn using six different κ_{nz} density profiles and the corresponding Γ_z impurity flux. The line's slope is equal to the diffusion coefficient D_z and its x-intercept/y-intercept yields respectively the peaking factor (PF) $-RV_z/D_z$ and the pinch velocity V_z . According to our notations, positive (negative) PF represents a peaked (hollow) impurity density profile and positive (negative) pinch velocity means particles move toward the edge (the core).

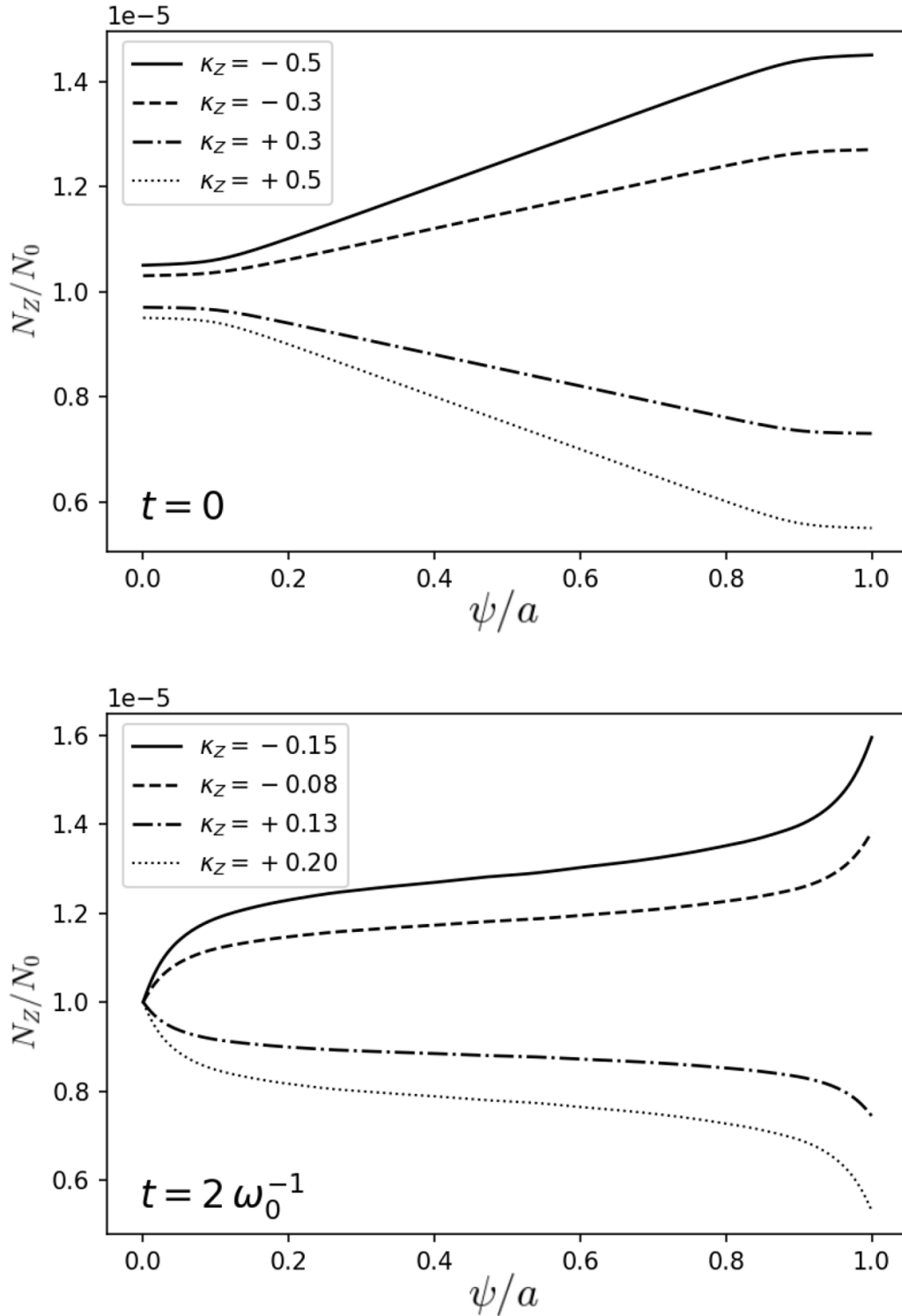


Figure 4. Impurity density profiles N_z with different initial values $\kappa_{nz} = \pm 0.3, \pm 0.5$. Initial density profiles at $t = 0$ (top) and measured density profiles at $t = 2\omega_0^{-1}$ (bottom) are shown.

Finding V_z values using a linear regression method with a restricted number of points ($\kappa_{nz}, \frac{\Gamma_z}{N_z}$) provides only an approximate value. It is, therefore, necessary to run several simulations with various κ_{nz} values to increase accuracy. In this study, 6 different values of κ_{nz} have been tested to calculate the value of V_z .

4. Parametric dependency of impurity pinch

Determining the complete parametric dependencies of impurity flux by non-linear gyrokinetic simulations is a demanding task. However, the bounce-averaged TERESA model only considers trapped particles (no parallel compressible pinch)

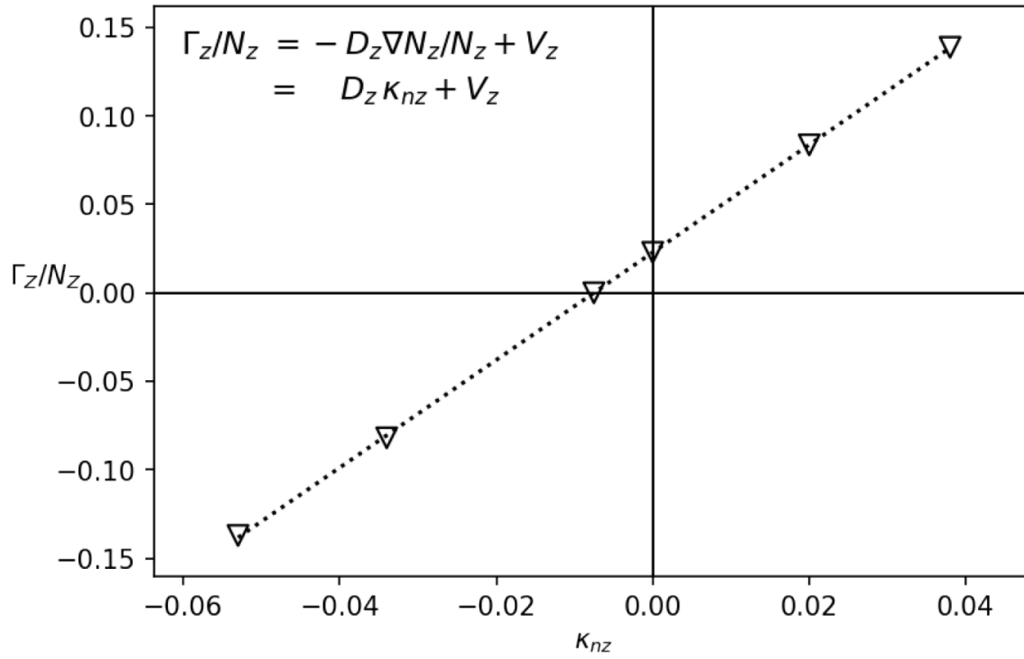


Figure 5. Example of linear relationship between density gradient and impurity particle flux.

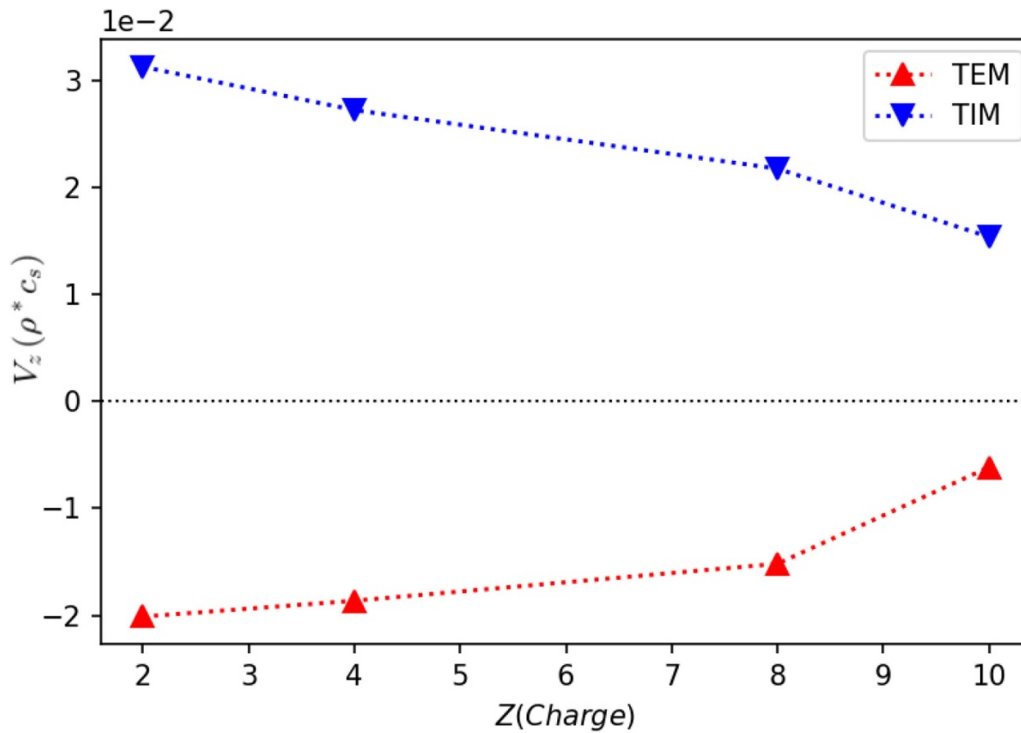


Figure 6. Direction of thermodiffusion and its charge dependency in TIM/TEM dominated plasma for a fixed impurity mass number $A = 20$. The coefficient C_T decreases in proportion to the impurity charge Z . For TEM, the thermodiffusion pinch flux is found to be inward, whereas it is found to be outward in the case of TIM turbulence.

and takes into account both thermodiffusion/curvature pinch. This reduced approach enables us to carry out an in-depth study into local parametric dependencies of convective terms in equation (15) by varying related parameters with considerably reducing numerical simulation time.

For the results shown in this paper, the parameters shown in table 4 such as the number of grid in the toroidal/radial/trapped parameter/energy direction $(N_\alpha, N_\psi, N_\kappa, N_E)$, the impurity concentration C_z and the zonal flows control parameter ϵ_ϕ are fixed during the entire work. The number of grid in κ is $N_\kappa = 1$

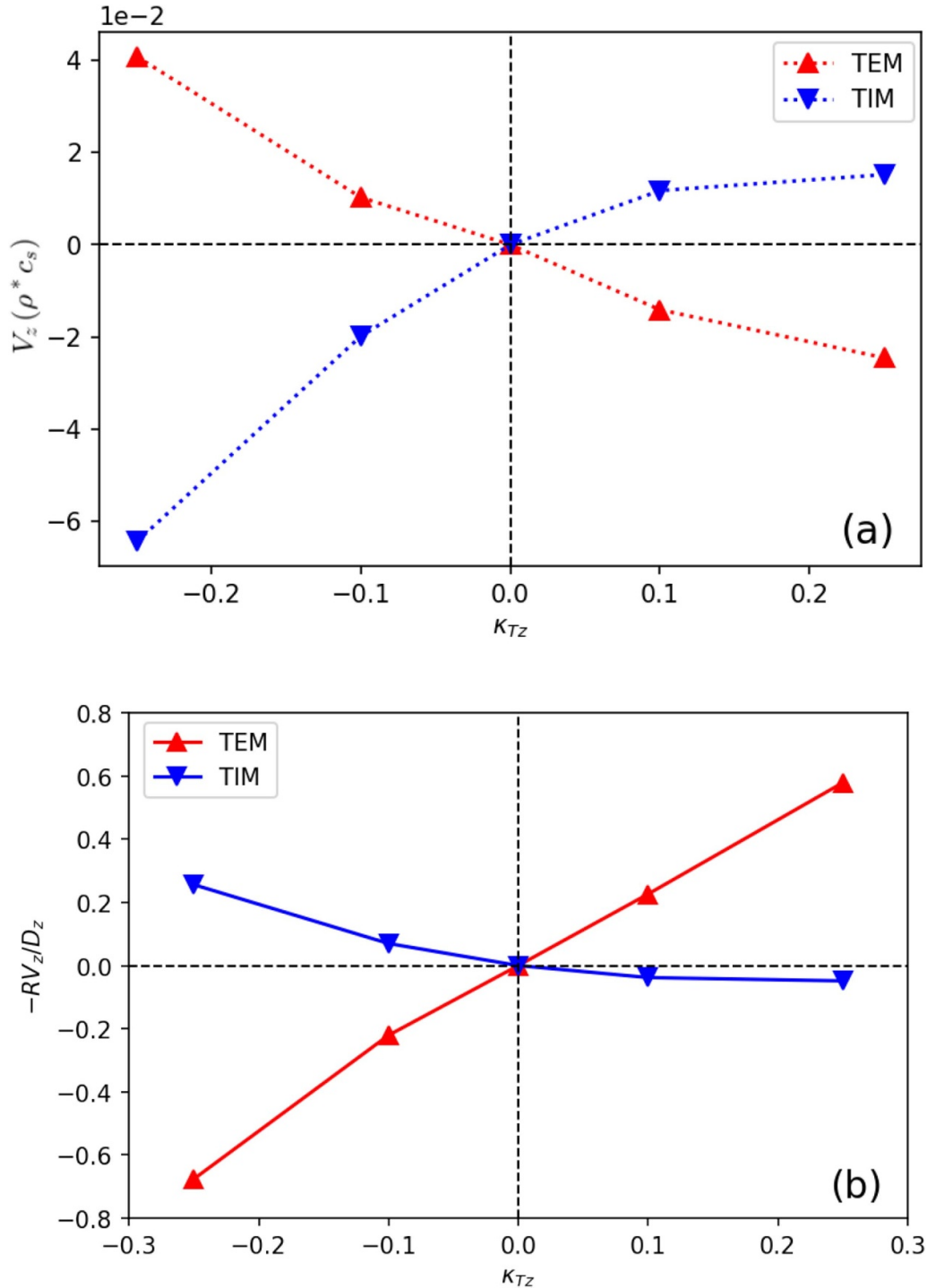


Figure 7. Thermodiffusion V_z (a) and normalized PF $-RV_z/D_z$ (b) plotted against κ_{Tz} , for both TEM and TIM turbulent cases.

Table 4. Plasma parameters.

N_α	N_ψ	N_κ	N_E	C_z	ϵ_ϕ
1024	256	1	96	10^{-5}	0.3

meaning that we consider strongly trapped particle only. These parameters remain unvaried unless otherwise mentioned.

Note that the impurity concentration $C_z = 10^{-5}$ is chosen in the trace limit ($N_z Z/N_i \ll 1$). Recently, the influence of

impurity concentration on the turbulence and the model itself has been investigated [34, 35]. However, in this paper, we restrict ourselves to the trace limit.

4.1. Thermodiffusion

First, the thermodiffusion term $C_T dT_{eq}/dr$ in the case of TIM/TEM has been studied with respect to its impurity charge. In order to get the thermodiffusion pinch exclusively, the

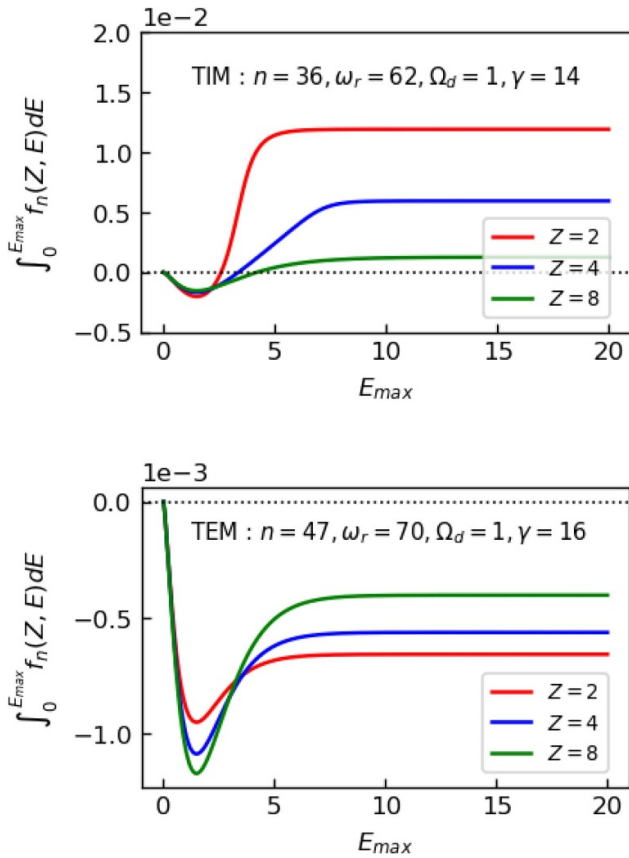


Figure 8. Thermodiffusion contribution $X_n(Z) = \int_0^{E_{max}} f_n(Z, E) dE$ in case of TIM/TEM using n, ω_r, γ obtained by linear analysis.

Table 5. Initial density/temperature profiles.

	κ_{ni}	κ_{ne}	κ_{Ti}	κ_{Te}	κ_{Tz}
TIM	0.1	0.1	0.2	0.05	0.05
TEM	0.1	0.1	0.05	0.2	0.05

curvature pinch C_p term has been removed. This can be achieved by putting $H_{eq} = E$ in the distribution function $f_{eq,s}$. As a result the last term in equation (14) disappears. The impurity mass number $A=20$ was kept unchanged while charge numbers $Z=2, 4, 8$ and 10 are tested. Initial density/temperature profiles for all species are listed in table 5:

For impurity density profiles, 8 points with different values of $\kappa_{nz} = \pm 0.05, \pm 0.1, \pm 0.3, \pm 0.5$ were chosen and their modified κ_{nz} value in turbulent region was used to find V_z as we explained in previous section. To differentiate TIM/TEM modes separately, different temperature gradients for ions/electrons have been used as background temperature profiles. Earlier fluid [7] and gyrokinetic models proposed that the sign of the coefficient C_T in equation (15) depends on the phase velocity of turbulence [26]. It is shown in figure 6 that the direction of thermodiffusion is outward (positive velocity V_z) in the case of TIM whereas it is inward (negative velocity V_z) when TEM dominates. This direction change can be

Table 6. Initial density/temperature profiles.

	κ_{ni}	κ_{ne}	κ_{Ti}	κ_{Te}	κ_{Tz}
TIM	0.1	0.1	0.2	0.05	$0.0, \pm 0.1, \pm 0.25$
TEM	0.1	0.1	0.05	0.2	$0.0, \pm 0.1, \pm 0.25$

Table 7. Initial density/temperature profiles.

κ_{ni}, κ_{ne}	κ_{Ti}	κ_{Te}	κ_{Tz}
0.1, 0.15, 0.2, 0.25	0.25	0.25	0.25

Table 8. Initial density/temperature profiles.

κ_{ni}	κ_{ne}	κ_{Ti}	κ_{Te}	κ_{Tz}	α
0.1	0.1	0.2	0.2	0	$0, \pm 0.5$

understood according to the electron or ion nature of the turbulence. When TIM dominates, the most unstable mode corresponds to H_{eq}/T_{eq} larger than $3/2$. On the other hand, it is lower than $3/2$ in case of TEM. According to equation (14), this different location of the most unstable mode leads to different directions of V_z . Also, C_T decreases with the charge number Z meaning that the thermodiffusion term will be less important in a high- Z impurity case such as tungsten(W).

Moreover, it has already been highlighted that the direction of impurity particle flux depends directly on the sign of impurity temperature profile κ_{Tz} [7]. To verify this local parametric dependence, the following density/temperature profiles are tested:

Five different values of impurity temperature profiles $\kappa_{Tz} = 0.0, \pm 0.1, \pm 0.25$ in the TIM/TEM modes have been tested to verify the velocity change in direction. According to equation (15), using the QL theory we obtained the impurity particle flux Γ_z that is thought to be perfectly diffusive when the impurity temperature profile is flat ($\kappa_{Tz} = 0$) in the case the curvature pinch is neglected ($H_{eq} = E$). These results are presented in figure 7. First, figure 7(a) shows the relation between the pinch velocity V_z and κ_{Tz} in the TIM/TEM modes. As we predicted, and outlined before, the pinch velocity disappears when $\kappa_{Tz} = 0$ which signifies that the impurity particle flux is perfectly diffusive and that V_z changes its sign when κ_{Tz} does. A positive value of κ_{Tz} means that the plasma core is hotter than the edge which corresponds to a realistic temperature profile for a future fusion scenario. In this case, the impurity pinch moves inward ($V_z < 0$) in the TEM mode whereas it moves outward ($V_z > 0$) in the TIM mode. This direction change according TIM/TEM instabilities can be explained from equation (14). Defining the function $f_n(Z, E)$ as follows,

$$f_n(Z, E) = \frac{\gamma}{(\omega_r - n \frac{\Omega_d}{Z} E)^2 + \gamma^2} \left(\frac{E}{T_{eq}} - \frac{3}{2} \right) \exp \left(-\frac{E}{T_{eq}} \right) \sqrt{E} \quad (23)$$

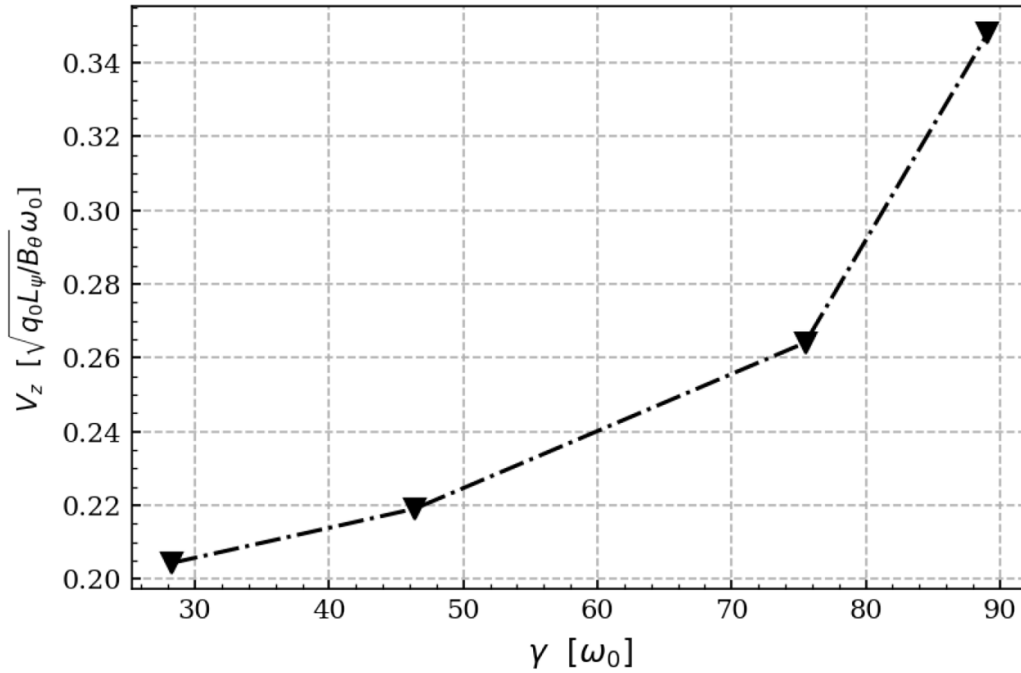


Figure 9. Pinch velocity V_z plotted against the linear growth rate γ .

we have the thermodiffusion which is proportional to

$$\sum_n \int_0^\infty (n \mathcal{J} \phi_n)^2 f_n(Z, E) dE \quad (24)$$

To see how this term varies with Z , we define a new function $X_n(Z) \equiv \int_0^\infty f_n(Z, E) dE$ and take its derivative with respect to Z to see how it changes with Z .

$$\frac{dX_n(Z)}{dZ} = - \int_0^\infty \frac{2\gamma n \Omega_d \frac{E}{Z^2} (\omega_r - n \Omega_d \frac{E}{Z})}{[(\omega_r - n \Omega_d \frac{E}{Z})^2 + \gamma^2]} \left(\frac{E}{T_{eq}} - \frac{3}{2} \right) \exp\left(-\frac{E}{T_{eq}}\right) \sqrt{E} dE \quad (25)$$

Assuming $T_{eq} = 1$ and $\omega_r \gg n \Omega_d$, we can further simplify equation (25).

$$\frac{dX_n(Z)}{dZ} = -1.33 \frac{2\gamma n \Omega_d \omega_r \frac{1}{Z^2}}{(\omega_r^2 + \gamma^2)^2} \quad (26)$$

Thus, the absolute value of $X_n(Z)$ decreases with Z in both cases TIM ($\omega_r > 0$) and TEM ($\omega_r < 0$). Note that this relation may fail to apply if the condition $\omega_r \gg n \Omega_d$ is not satisfied. To verify this limit in the case of our numerical simulations, linear analysis has been performed to find the most unstable mode number n and the corresponding values of ω_r, γ according to the plasma parameters. In figure 8, $X_n(Z)$ is calculated with different impurity charges. The background profiles from table 5 have been used to obtain n, ω_r, γ and Ω_d is equal to 1 since all the frequencies are normalized to the ion precession frequency. The values of n, ω_r and γ are displayed in figure 8, and we can see that equation (26) works in both TIM/TEM

case even though $\omega_r \gg n \Omega_d$ is roughly assured (factor $\simeq 2$) and the thermodiffusion is inversely proportional to impurity charge.

Here, the same order of magnitude for TIM/TEM convection is found in figure 7(a). Although the TIM instability plays minor role in impurity transport compared with other main instabilities such as ITG and TEM, our investigations must be taken as a qualitative analysis of transition between ion-driven and electron-driven instabilities in general. Furthermore, our model considers only trapped particles where ITG cannot be investigated.

In figure 7(b), the normalized PFs $-RV_z/D_z$ are depicted as a function of $\kappa_{T,z}$. Since the PF sign inversely depends on the sign of V_z , PF exhibits the opposite behavior as V_z . Here, a negative PF signifies hollow impurity density profile and positive PF means peaked impurity density profile to be avoided for the efficiency of fusion. Consequently, in the general plasma fusion scenario where the core is hotter than the edge (positive $\kappa_{T,z}$ in figure 7), the electron dominant mode will accumulate impurities in the core while ion dominant regime will pump out impurities toward the edge [7, 10].

To date, the thermodiffusion direction has been particularly investigated. In this section, we aim to determine the magnitude of the C_T coefficient with respect to the intensity of the background plasma turbulence. Since we are only interested in the absolute value of V_z with respect to turbulence intensity, ion and electron temperature profiles have been chosen arbitrarily without considering TIM or TEM dominance. Detailed density/temperature profiles are listed below:

While keeping the temperature gradient constant for $s = i, e, z$, main ion and electron density gradients have been gradually increased from $\kappa_{ni} = \kappa_{ne} = 0.1$ to 0.25. To compare the turbulence intensity with the pinch velocity V_z ,

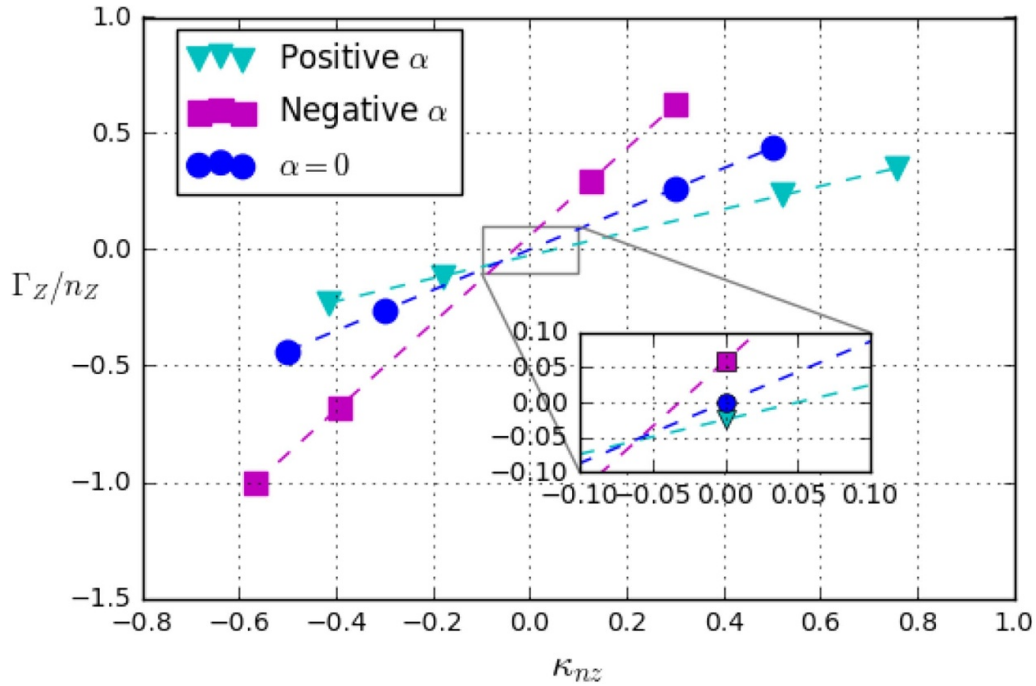


Figure 10. Γ_z/n_z plotted against κ_{nz} , with different coefficient values α in $H_{eq} = E(1 + \alpha e\Omega_d\psi)$. The thermodiffusion term is removed by considering the case $\kappa_{Tz} = 0$.

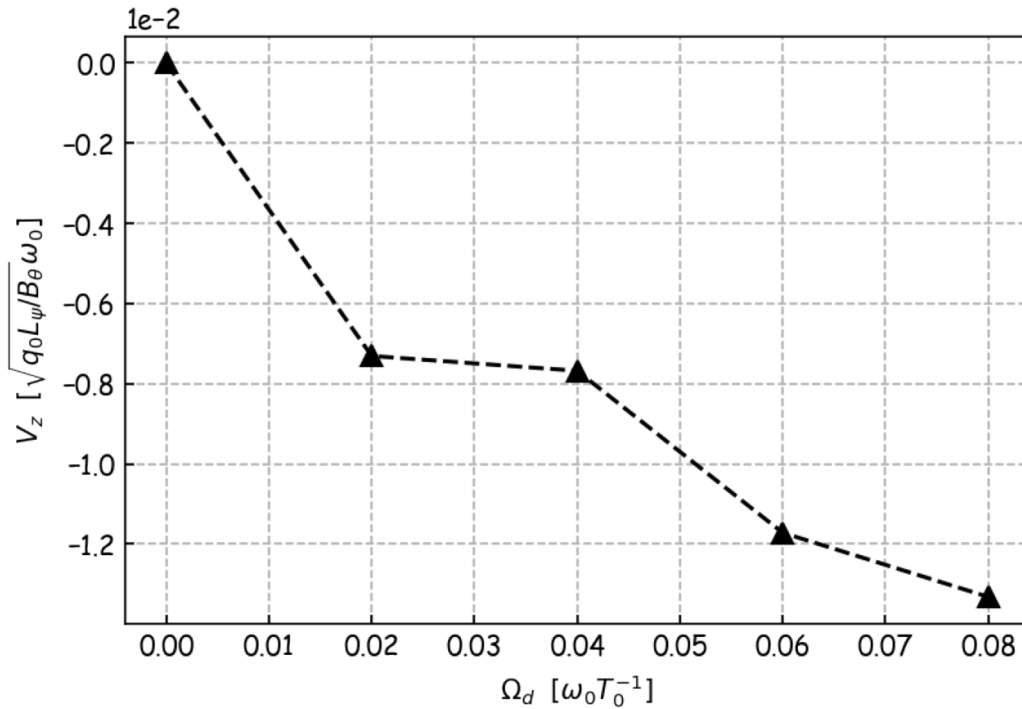


Figure 11. Pinch velocity V_z plotted against Ω_d .

the growth rate γ and the ϕ spectrum have been computed (figure 3(a)).

It is shown in figure 9 that the absolute value of V_z increases with the growth rate γ . The more a plasma is turbulent, the stronger the observed pinch. This result was expected because the turbulent transport is proportional to $|\phi|^2$ and this increases with the growth rate γ (see equation (14)).

4.2. Curvature pinch

In the previous section, the thermodiffusion was studied by neglecting the magnetic curvature in the distribution function f_{eq} . In this paragraph, the flat impurity temperature profile $\kappa_{Tz} = 0$ is imposed while the entire Hamiltonian $H_{eq} = E(1 + e\Omega_d\psi)$ is taken into account.

From equation (14), it appears that the direction of curvature pinch relies on the sign of Ω_d ($\Omega_d = \frac{Z_s \omega_{d,s}}{E}$). In the general case, Ω_d depends in a complicated manner on the trapping parameter and on the magnetic shear (cf. equation (2)). As already stated, it is mostly positive for trapped particles, except close to the trapped/passing boundary and/or for negative magnetic shear [24]. In our simplified approach where only deeply trapped particles are considered, it is a positive constant. So as to nevertheless explore its impact on the pinch curvature while still relying on our simplification, we introduce the ad-hoc parameter α so as to control both the sign and magnitude of the normalized precession frequency Ω_d . The equilibrium Hamiltonian then reads $H_{eq} = E(1 + \alpha e \Omega_d \psi)$, with $\alpha = \{0, \pm 1/2\}$ in the considered simulations. Note that $\alpha > 0$ corresponds to the usual sign of Ω_d for trapped particles, while $\alpha < 0$ would mimic the expected situation for strong negative magnetic shear or near the trapped/passing boundary. Then we use the same linear approach as in figure 5 to find the pinch velocity. The following density profiles are tested for different values of α :

The direction of the curvature pinch velocity V_z with different values of α is represented in figure 10. As we expected from equation (14), for the usual sign of precession frequency (positive α) the curvature pinch velocity V_z is always inward. In contrast, the strong negative magnetic shear s_0 (negative α) can switch the sign of V_z , then it pushes the impurity particle toward the edge. The $\alpha = 0$ case corresponds to no magnetic curvature. Therefore, the impurity flux is purely diffusive and the linear line Γ_z/n_z passes exactly the origin point ($V_z = 0$).

Finally, to illustrate the impact of α over the magnitude of V_z , we choose to run several cases while keeping α positive. The magnitude of V_z as a function of Ω_d is shown in figure 11. The increase of V_z with respect to Ω_d is consistent with our QL model (equation (14)).

It should be noted that the curvature pinch term sometimes prevails over the thermodiffusion term. But, in this paper, we search for the parametric tendency of impurity pinch terms, not their exact physical value, so the curvature pinch V_z is of the same order of the thermodiffusion pinch.

5. Conclusion

In this paper, the parametric dependencies of impurity pinch caused by trapped particle driven turbulence were studied using the bounce-averaged gyrokinetic code TERESA. With this reduced model, the thermodiffusion and the curvature pinch terms were both investigated by comparison with QL theory. The Kubo number was computed for the validity of QL framework and it was found that the QL approximation is valid in case of weakly unstable plasma. The parametric dependencies of convective terms were shown with respect to other parameters such as $\nabla n_{i,e}/n_{i,e}$, $\nabla T_{i,e}/T_{i,e}$, $\nabla T_z/T_z$, impurity charge Z and magnetic shear s_0 . For all simulations, light impurities in the trace limit have been kept.

First, the sign of thermodiffusion coefficient C_T was investigated in the case of TIM/TEM turbulence separately. The results obtained from non-linear simulations are in agreement

with previous papers [7, 16] and the QL theory, confirming that the impurities move inward in the case of TEM turbulence and outward in the case of TIM turbulence. This can be explained by different energy resonance position in the case of TIM/TEM. It is also found that the magnitude of C_T decreases with impurity charge Z but the coefficient C_T might be important in strong turbulent regime.

Secondly, the curvature pinch was investigated with respect to the magnetic curvature. In general, regardless of the background plasma turbulence, the curvature pinch is inward except in the case of a strongly reversed magnetic shear. We found that our numerical simulation reproduces the same trend with the QL theory. It is also found that the magnitude of the curvature pinch is proportional to magnetic shear s_0 .

A clear understanding of impurity dynamics for further work would require more sophisticated model, including a collision operator, realistic tokamak geometry, magnetic perturbation, etc. However, the limited computing performance at the current time precludes us from reaching this level. In this context, the bounce-averaged gyrokinetic TERESA code provided us with corresponding outputs about impurity dynamics with reasonable computation time and we also showed that these results in qualitative agreement with our kinetic QL model.

Acknowledgments

The authors thank the referees for their helpful comments and their input. This work was carried out within the framework of the French Federation for Magnetic Fusion Studies (FR-FCM) and of the Eurofusion consortium. It received funding from the Euratom research and training programme 2014–2018 and 2019–2020 under grand agreement No 633053. The views and opinions expressed herein do not necessarily reflect those of the European Commission.

This work was granted access to the HPC resources of IDRIS under the allocation 2019 made by GENCI-IDRIS (Grand Equipement National de Calcul Intensif).

Appendix A. Quasi-linear impurity transport by fluid approach

In this appendix, the impurity particle flux Γ_z is derived by fluid approach of the quasi-linear theory. This approach gives the same results as those presented in section 3.1 and the presence of diffusive and convective part are expressed below.

First, the bounce-averaged distribution function f_s satisfies the Vlasov equation (equation 1):

$$\frac{\partial f_s}{\partial t} - [\mathcal{J}\phi, f_s] + \frac{E\Omega_d}{Z_s} \frac{\partial f_s}{\partial \alpha} = 0 \quad (\text{A1})$$

The first and second moment of equation (A1) then leads to the time evolution of the density and pressure terms respectively.

$$\frac{\partial N}{\partial t} + \frac{\partial \bar{\phi}}{\partial \psi} \frac{\partial N}{\partial \alpha} - \frac{\partial \bar{\phi}}{\partial \alpha} \frac{\partial N}{\partial \psi} + \frac{3}{2} \frac{\Omega_d}{Z_s} \frac{\partial p}{\partial \alpha} = 0 \quad (\text{A2})$$

$$\frac{\partial p}{\partial t} + \frac{\partial \bar{\phi}}{\partial \psi} \frac{\partial p}{\partial \alpha} - \frac{\partial \bar{\phi}}{\partial \alpha} \frac{\partial p}{\partial \psi} + \frac{5}{2} \frac{\Omega_d}{Z_s} \frac{\partial}{\partial \alpha} (pT) = 0 \quad (\text{A3})$$

Here, $\bar{\phi}$ represents the gyro-bounce averaged potential. This notation will be omitted from now on for reason of brevity.

Using the linearization in the Fourier space $\bar{\phi} = \sum_l \phi_l(\psi, t) e^{il\alpha}$ and $\tilde{N}_s = \sum_l N_l(\psi, t) e^{il\alpha}$, equations (A2) and (A3) become:

$$-i\omega N_l + il \frac{3}{2} \frac{\Omega_d}{Z_s} (T_l N_{eq} + N_l T_{eq}) - il \phi_l \frac{\partial N_{eq}}{\partial \psi} = 0 \quad (\text{A4})$$

$$\left(-i\omega T_{eq} + il \frac{5}{2} \frac{\Omega_d}{Z_s} T_{eq}^2 \right) N_l + \left(-i\omega N_{eq} + il \frac{5\Omega_d}{Z_s} N_{eq} T_{eq} \right) T_l - il \phi_l \frac{\partial p_{eq}}{\partial \psi} = 0 \quad (\text{A5})$$

After some arrangement, above two equations can be rewritten:

$$\frac{2\omega}{3l\Omega_d/Z_s} N_l + \frac{2l}{3\Omega_d/Z_s} \phi_l \frac{\partial N_{eq}}{\partial \psi} = T_l N_{eq} + N_l T_{eq} \quad (\text{A6})$$

$$(\omega - \omega_T) T_{eq} N_l + l \phi_l \frac{\partial p_{eq}}{\partial \psi} + (\omega - 2\omega_T) N_{eq} T_l = 0$$

Here, we replaced $5l\Omega_d T_{eq}/2Z_s$ term by ω_T . Further arrangement leads to finally:

$$\frac{T_l}{T_{eq}} = \left(\frac{5\omega}{3\omega_T} - 1 \right) \frac{N_l}{N_{eq}} + \frac{5l\hat{\phi}}{3\omega_T} \frac{1}{N_{eq}} \frac{\partial N_{eq}}{\partial \psi}$$

$$(\omega - \omega_T) \frac{N_l}{N_{eq}} + l \phi_l \frac{1}{\underbrace{\frac{\partial p_{eq}}{\partial \psi}}_{\kappa_{neq} + \kappa_{Teq}}} + (\omega - 2\omega_T) \frac{T_l}{T_{eq}} = 0 \quad (\text{A7})$$

Combining above two equations gives follow result:

$$\left[(\omega - \omega_T) \omega_T + (\omega - 2\omega_T) \left(\frac{5\omega}{3} - \omega_T \right) \right] \frac{N_l}{N_{eq}} = \left[(\kappa_{neq} + \kappa_{Teq}) \omega_T + \frac{5}{3} (\omega - 2\omega_T) \kappa_{neq} \right] (-l\phi_l) \quad (\text{A8})$$

where the density/temperature profile $\kappa_{n,T_{eq}}$ is defined as $\kappa_{n,T_{eq}} = \partial_\psi \log(N_{eq}, T_{eq})$. Averaging equation (A2) over α gives the impurity particle flux Γ_z according to the continuity equation.

$$\frac{\partial N_s}{\partial t} + \frac{\partial \Gamma_s}{\partial \psi} = \frac{\partial N_s}{\partial t} - \frac{\partial}{\partial \psi} \left\langle \frac{\partial \bar{\phi}}{\partial \alpha} N_s \right\rangle = 0 \quad (\text{A9})$$

Now, the particle flux Γ_z can be written:

$$\Gamma = - \left\langle \frac{\partial \bar{\phi}}{\partial \alpha} \tilde{N} \right\rangle = - \left\langle \sum_l il \phi_l e^{il\alpha} \sum_l N_l e^{il\alpha} \right\rangle = i \sum_l l N_l \phi_l^* \quad (\text{A10})$$

Knowing the relation between perturbed potential and density, we insert equation (A8) into equation (A10). After some

arrangement, the particle flux in the TERESA model can finally be written as follows:

$$\Gamma = i \sum_l N_{eq} (-l\phi_l) (l\phi_l^*) \frac{(\kappa_{neq} + \kappa_{Teq}) \omega_T + \frac{5}{3} (\omega - 2\omega_T) \kappa_{neq}}{(\omega - \omega_T) \omega_T + (\omega - 2\omega_T) \left(\frac{5}{3} \omega - \omega_T \right)}$$

$$= -i \sum_l \frac{N_{eq} l^2 |\phi_l|^2}{(\omega - \omega_T) \omega_T + (\omega - 2\omega_T) \left(\frac{5}{3} \omega - \omega_T \right)}$$

$$\left[\frac{1}{3} (5\omega - 7\omega_T) \kappa_{nz} + \omega_T \kappa_{Tz} + \frac{5\Omega_d}{2} \frac{\omega - \omega_T}{1 + \Omega_d \psi} \right] \quad (\text{A11})$$

where we put $N_l = \frac{N_{eq}}{(1 + \Omega_d \psi)^{3/2}}$ and $T_l = \frac{T_{eq}}{(1 + \Omega_d \psi)}$ for perturbed density/temperature, so $\kappa_{neq}, \kappa_{Teq}$ was replaced by $\kappa_{neq} = \kappa_n + \frac{3\Omega_d}{2(1 + \Omega_d \psi)}$ and $\kappa_{Teq} = \kappa_T + \frac{\Omega_d}{(1 + \Omega_d \psi)}$.

The complex form of Γ_z in equation (A11) can be simplified by binding all the terms with respect to κ_n and κ_T separately, and the equation can be rewritten as follows:

$$\Gamma_z \sim D \kappa_{nz} + C_T \kappa_{Tz} + C_P \quad (\text{A12})$$

The first term which is proportional to κ_{nz} corresponds to the diffusive term and the second term which is proportional to impurity temperature gradient κ_{Tz} is the thermodiffusion term. And the last term is the curvature pinch term coming from magnetic curvature.

ORCID iDs

K Lim  <https://orcid.org/0000-0002-0174-2300>
 E Gravier  <https://orcid.org/0000-0002-8911-5546>
 X Garbet  <https://orcid.org/0000-0001-5730-1259>
 Y Sarazin  <https://orcid.org/0000-0003-2479-563X>

References

- [1] Philipps V 2011 *J. Nucl. Mater.* **S2-S9** 415
- [2] Putterich T et al 2010 *Nucl. Fusion* **50** 025012
- [3] Isichenko M B, Gruzinov A V and Diamond P H 1995 *Phys. Rev. Lett.* **74** 4436
- [4] Dimits A M et al 2000 *Phys. Plasmas* **7** 969
- [5] Angioni C et al 2015 *Phys. Plasmas* **22** 055902
- [6] Casson F J et al 2010 *Phys. Plasmas* **17** 102305
- [7] Dubuit N et al 2007 *Phys. Plasmas* **14** 042301
- [8] Nordman H et al 2011 *Plasma Phys. Control. Fusion* **53** 105005
- [9] Skyman A et al 2015 *Nucl. Fusion* **54** 013009
- [10] Angioni C and Peeters A G 2006 *Phys. Rev. Lett.* **96** 095003
- [11] Estrada-Mila C, Candy J and Waltz R E 2005 *Phys. Plasmas* **12** 022305
- [12] Camenen Y et al 2009 *Phys. Plasmas* **16** 012503
- [13] Angioni C et al 2011 *Nucl. Fusion* **51** 023006
- [14] Casson F J et al 2015 *Plasmas Phys. Control. Fusion* **57** 014031
- [15] Donnel P et al 2019 *Plasma Phys. Control. Fusion* **61** 014003
- [16] Guirlet R et al 2006 *Plasma Phys. Control. Fusion* **48** B63
- [17] Esteve D et al 2018 *Nucl. Fusion* **58** 036013
- [18] Sonnendrucker E, Roche J, Bertrand P and Ghizzo A 1999 *J. Comput. Phys.* **149** 201
- [19] Depret G et al 2000 *Plasmas Phys. Controlled Fusion* **42** 949
- [20] Sarazin Y et al 2005 *Plasmas Phys. Control. Fusion* **47** 1817
- [21] Lesur M et al 2017 *Phys. Plasmas* **24** 012511

- [22] Drouot T *et al* 2014 *Eur. Phys. J. D* **68** 280
[23] Cartier-Michaud T *et al* 012003 *J. Conf. Ser.* **561** 2014
[24] Kadomtsev B B and Pogutse O P 1967 *Soviet Phys. JETP* **24** 1172
[25] Futatani S, Garbet X, Benkadda S and Dubuit N 2010 *Phys. Rev. Lett* **104** 015003
[26] Bourdelle C *et al* 2007 *Phys. Plasmas* **14** 112501
[27] Eriksson A *et al* 2005 *Phys. Plasmas* **12** 092509
[28] Gravier E *et al* 2019 *Phys. Plasmas* **26** 082306
[29] Medina J *et al* 2018 *Phys. Plasmas* **25** 122304
[30] Coppi B and Spight C 1978 *Phys. Rev. Lett.* **41** 551
[31] Kubo R 1963 *J. Math. Phys.* **4** 174
[32] Ottaviani M 1992 *Europhys. Lett.* **20** 111
[33] Shalchi A 2016 *New J. Phys.* **18** 085010
[34] Idouakass M *et al* 2018 *Phys. Plasmas* **25** 062307
[35] Lesur M *et al* 2020 *Nucl. Fusion* **60** 036016